Green Chemistry

Accepted Manuscript

ROYAL SOCIETY OF CHEMISTRY

www.rsc.org/greenchem

Hierarchical micro-/mesoporous N- and O-enriched carbon derived from disposable cashmere: A competitive cost-effective material for high-performance electrochemical capacitors

Lu Zhou [a], *Hui Cao* [a], *Siqi Zhu* [a], *Linrui Hou* [a] *and Changzhou Yuan* *[a, b]

[a] *School of Materials Science & Engineering, Anhui University of Technology, Ma'anshan, 243002, P.R. China*

E-mail: ayuancz@163.com

[b] *Chinese Academy of Science (CAS) Key Laboratory of Materials for Energy Conversion, Hefei, 230026, P.R. China*

Abstract

To obtain advanced carbon materials for next-generation electrochemical capacitors (ECs), it is critical to understand the synergetic effect of versatile carbon surface functionalities and specific pore structure on their electrochemical performance. Herein, we developed a facile yet scalable fabrication of N- and O-enriched carbon with nanoscale to mesoscale porous structures from the disposable cashmere. The hierarchical cashmere-derived micro-/mesoporous carbon (CDMMC) was endowed with desirable specific surface area (SSA, 1358 m^2 g^{-1}), hierarchical porosity with high microporosity of ~45.5%, and high content of heteroatom functionalities (~4 at.% N and ~15.5 at.% O). Even better electrochemical capacitance of the resultant CDMMC was obtained in 1 M H_2SO_4, benefiting from the hierarchical micro-/mesoporosity, large effective SSA and remarkable heteroatom (N, O) doping effects, that is, the smart combination of double layer and Faradaic contributions, compared to that in KOH. Furthermore, larger energy density (~17.9 Wh kg^{-1}) of the CDMMC-based symmetric device was obtained with organic electrolyte, in contrast to those with aqueous electrolytes.

Key Words: N- and O-enriched carbon; Hierarchical porosity; Faradaic contributions; Cashmere; Electrochemical capacitors

1. Introduction

In response to the tremendous demands of modern society and emerging ecological concerns, it is now essential and urgent to explore new, low-cost and environmentally friendly electrochemical energy storage systems (EESSs).[1-3] Electrochemical capacitors (ECs, also called supercapacitors), as an intriguing one at the forefront of the available EESSs, have attracted enormous interest so far, thanks to their better rate capability and longer cyclic life as compared to secondary batteries.[1, 2, 4, 5] And they has been used widely as power sources for versatile applications requiring quick bursts of energy, such as high-power electronic devices, electric vehicles (EVs), hybrid EVs, and so on. According to established charge-storage mechanisms coupled with the utilized electroactive materials, ECs are generally categorized into pseudo-capacitors and electric double-layer capacitors (EDLCs).[4] The former primarily originates from fast reversible Faradaic reactions at the electrode (such as, metal oxides/sulfides,[6, 7] conducting polymers,[8] *etc.*)/electrolyte interfaces under certain potentials. And the latter stores electrochemical energy based on the electrosorption of electrolyte molecules/ions on the surface of the carbonaceous electrodes.[3-5] It is owing to their higher power densities and longer cycle life than pseudo-capacitors that EDLCs stand out from EESSs. Unfortunately, this is at the expense of considerably low energy density meanwhile.[4, 5, 9] As a result, immense interest and efforts have been extensively triggered to explore and develope optimum carbon materials that can be applied practically as advanced electrodes to deliver large pulse current and high energy density simultaneously.

As established well, carbon materials with remarkable specific capacitances (SCs) are commonly those who own large specific surface area (SSA), hierarchical porous architecture (*i.e.*, micropores and mesopores), and high surface heteroatom (such as O, N, B, P, *etc.*)[9-18] content. In specific, large SSA imparts rich electroactive sites for efficient charge accommodation and/or occurrence of sufficient redox reactions.[9] The hierarchical micro-/mesopores provide large SSA, and meanwhile, the mesopores can further serve as ion highways allowing for very fast ion transport into the bulk of the electrode, thus ensuring high power density.[9, 11-16] The introduced

foreign atoms render the acid/case properties to the carbon, and typically contribute the extra pseudo-capacitance from the striking redox process of the surface heteroatom functionalities.[3, 10-15, 17] In particular, N- and O-based functional groups also can improve the wettability between carbon surface and electrolyte solution by the formation of polar functional groups, enhancing the interaction between the carbon electrodes and electrolytes.[17, 19] Among these heteroatoms, N element is especially a very promising candidate, benefiting from its high electronegativity, small atomic diameter, and additional free electrons contributing to the conduction band of carbons, which make the N-doped carbon better electronic conductivity compared to their pure counterparts.[3, 10-13, 15] Therefore, the N- and O-doped carbon frameworks with hierarchical porosity, combining both of the advantages including indefinitely reversible double-layer capacitance at the electrode/electrolyte interfaces and the rapid, and reversible pseudo-capacitance, would be better candidates for advanced EC with higher energy density and power property meantime. Furthermore, intensively exploring and broad utilization of the relatively cheap precursors and/or universal resources, particularly some biomass waste materials obtained directly in nature for the smart fabrication of hierarchical porous N- and O-doped carbon materials, would be of great benefit to their large-scale synthesis and widespread ECs applications. More significantly, N- and O-enriched carbons can be prepared by directly pyrolyzing biomass that is naturally rich in these elements, which greatly favors for a more homogeneous incorporation of the N and/or O species into the bulk, rather than just on their surfaces with controlled chemistry.[19] For instance, functionalized carbons with appealing electrochemical characteristics have been recently obtained from gelatin,[20] bacteria,[13] dead leaves,[21] human hairs,[12] animal bones, [21, 23] fish scale, [24, 25] banana fibers,[26] rice husk,[27] catkins,[28] big bluestem,[29] enteromorpha prolifera,[30] and so on.

With these comprehensive considerations in mind, we herein put forward a facile yet scalable bio-inspired synthesis of N- and O-functionalized carbon material with nanoscale to mesoscale porous structures by using disposable cashmere source as raw material. The cost-effective cashmere was chosen as the precursor mainly based on the following facts: (I) Cashmere largely composed of

keratin amino acids is one of the unique renewable natural material with highly N-contained components; (II) Facile fabrication of commercially available functionalized carbon from abundant and biomass residues can meet the rigorous demand of effective industrial production. Furthermore, the resulting hierarchical cashmere-derived micro-/mesoporous carbon (henceforth denoted as CDMMC) was endowed with a large SSA of 1358 m^2 g^{-1}, hierarchical porosity of 1.23 cm^3 g^{-1} with high microporosity of 45.5 %, and high content of heteroatom functionalities (N of ~4 at.% and O of ~15.5 at.%). It was the prominent synergy of these structural and compositional advantages that imparts exquisite electrochemical performance to the as-fabricated hierarchical CDMMC material both in aqueous and organic electrolytes. In addition, superior electrochemical properties were observed for the CDMMC electrode in 1 M H_2SO_4, owing to the micro-/mesoporosity coupled with large effective SSA and striking heteroatom-doping effects, *i.e.*, elegant combination of double layer and Faradaic contributions, compared to that in 6 M KOH. Furthermore, larger specific energy density (SED) is obtained by the CDMMC-based symmetric EC with an aprotic electrolyte of tetraethylammonium and tetrafluoroborate in propylene carbonate (hereafter designed as $TEABF_4$/PC). The excellent supercapacitive performance encourages its aspired commercial exploitation for the development of advanced ECs. More significantly, the strategy we developed here opened up the great possibility of synthesizing sustainable and cost-effective materials for next-generation ECs.

2. Experimental Section

Materials synthesis The disposed cashmere (Neimenggu, China) was thoroughly washed with de-ionized (DI) water and dried at 80 °C. The cleaned cashmere was first pyrolyzed in a tubular furnace at a temperature of 300 °C for 2 h with a heating rate of 5 °C min^{-1} under high-purity N_2 atmosphere. During the following KOH-activated process, the as-obtained black powder was further mixed with activation agent KOH in a KOH/pre-pyrolyzed carbon ratio of 3 : 1 (W/W). Afterwards, the mixture was activated under N_2 flow at 800 °C for 2 h in a tubular furnace with a heating rate of 3 °C min^{-1}. After completion of the activation, the sample was allowed to cool to

room temperature (RT). The resultant material was further purified in 0.1 M HCl solution, rinsed with DI water until neutral, and then dried in vacuum at 80 °C. The tap density of the as-obtained sample is ~0.3 g cm^{-3}. And the yield of the CDMMC sample is ~58%.

Materials characterization The morphologies and structures of the resulting samples were examined by field-emission scanning electron microscopy (FESEM, JEOL-6300F, 15 kV), transmission electron microscope (TEM), high-resolution TEM (HRTEM) (JEOL JEM 2100 system operating at 200 kV). N_2 adsorption/desorption was determined by Brunauer-Emmett-Teller (BET) measurement by using an ASAP-2020 surface area analyzer. The mesopore size distribution was derived from the adsorption branch of the Barrett-Joyner-Halenda (BJH) method, and the micropore size distribution was estimated by the Horvanth-Kawazoe (HK) method. X-ray photoelectron spectroscopy (XPS) measurement was performed on a PHi5000 X-ray photoelectron spectrometer with an Al K*a* excitation source (1486.6 eV), the spectra were fitted with the XPSPEAK41 software. Before XPS analysis, the sample was dried at 120 ºC in vacuum oven overnight to remove the absorbed water. The Raman analysis of the sample was recorded by laser Raman (T6400, Jobion yzon Crop. France). The contact angle was obtained on a video contact angle instrument (OCA 15+, Dataphysics). A round CDMMC tablet was obtained by pressing (~20 MPa) 30 mg of the obtained mesoporous CDMMC by using a tablet compression machine. And the thickness and diameter of the round tablet were measured by a vernier caliper. The as-fabricated round CDMMC tablet was further used for the electronic conductivity measurement by a four-point probe meter (SDY-5, Guangzhou, China) at RT.

Electrochemical tests The working electrode was prepared with the electroactive material CDMMC, acetylene black (AB) and polytetrafluoroethylene (PTFE) in a weight ratio of 8 : 1 : 1. A small amount of DI water was then added to make more homogeneous mixture, which was pressed onto a nickel foam (1 cm^2) current collector at a pressure of 15 MPa for following electrochemical measurements in 6 M KOH solution. The mixture was also smeared onto the pretreated graphite substrate[31] (1 cm^2) instead for electrochemical characterization in 1 M H_2SO_4 aqueous electrolyte.

The typical loading of the electroactive CDMMC is 3 mg cm^{-2} for the electrochemical evaluation in both the two electrolytes. Electrochemical characterizations were performed in three-electrode systems, where a platinum plate (1 cm^2) and a saturated calomel electrode (SCE) were used as the counter and reference electrodes, respectively, or two-electrode configure by using two identical electrodes face to face in 6 M KOH (or 1 M H_2SO_4) electrolyte.

In addition, a CDMMC-based symmetric EC was also electrochemically characterized in a aprotic electrolyte of 1 M $TEABF_4$/PC (Honeywell Corp.). The electrode was prepared by mixing 80 wt.% CDMMC material, 10 wt.% AB and 10 wt.% polyvinylidene difluoride (PVDF) binder dispersed in the N-methylpyrrolidinone (NMP). The slurries were coated on the Al foil and steel foil, which were employed as positive and negative current collectors, respectively. After coating, the electrodes were dried at 100 °C for 30 min to remove the solvent before pressing. The electrodes were further dried in vacuum at 120 °C for 24 h, and weighted. The typical mass loading of the CDMMC was 1.2 mg per Al foil (or Cu foil). The two symmetrical electrodes were separated by using a separator with the electrolyte of 1 M $TEABF_4$/PC in a CR2032 coin-type cell.

Electrochemical performance was evaluated by cyclic voltammetry (CV), chronopotentiometry (CP) and electrochemical impedance spectroscopy (EIS) measurements performed with an IVIUM electrochemical workstation (the Netherlands). The cycling performance was carried out with a CT2001D tester (Wuhan, China). The SCs of the electrode or symmetric ECs were calculated from the CP curves based on the following equation:

$$SC = \frac{It}{\Delta V} \qquad (1)$$

where I, t and ΔV were the discharging current density (A g^{-1}), the discharging time (s) and the discharging potential range (V) of the electrode or symmetric EC, respectively. Of note, the I was calculated based on the two identical electrodes for the case of symmetric ECs. Another important parameter, coulombic efficiency (CE), can be evaluated from the equation (2):

$$CE = \frac{t_D}{t_C} \times 100\% \quad (2)$$

where t_D and t_C are the time for galvanostatic discharging and charging, respectively.

And the *SED* and specific power density (*SPD*) of the CDMMC-based symmetric ECs in aqueous or organic electrolytes can be calculated by using the following equations:[14, 21, 32, 33]

$$SED = \frac{1}{2} SC(\Delta V)^2 \quad (3)$$

$$SPD = SED / t \quad (4)$$

where *SC* is the capacitance of the symmetric device calculated based on the mass of the electroactive CDMMC in the two electrodes. And the ΔV is for the working potential window of the CDMMC-based symmetric ECs.

3. Results and discussion

3.1 Physicochemical characterization

In our synthetic strategy, two procedures involving in the pre-carbonization and following activation process were carried out for the efficient fabrication of hierarchical porous CDMMC material, as schematically illustrated in **Fig. 1a**. The cleaned and dried cashmere fibers were pre-carbonized at a temperature of 300 ºC for 1 h. The as-pretreated carbon was then mixed homogeneously with KOH (1 : 3 in weight), and further carbonized at 800 ºC. As one of most frequently used activation strategies in industry, the activation temperature applied in the KOH activation of carbon materials is of great significance. In general, low-temperature (500 – 700 ºC) activation mainly generate micropores, and high-temperature activation (700 – 1000 ºC) will broaden the PSD through the formation of additional mesopores but accelerate the nitrogen loss meanwhile.[17, 34, 35] Thus, our primary consideration for employing a moderate activation temperature of 800 ºC here is to preserve the N-functionalities as many as possible, in addition to maximizing the ion accessible porosity and ensuring large SSA meantime.

Raman spectrum and corresponding fitted data of the resultant hierarchical CDMMC sample are depicted in **Fig. 1b**. The spectrum shows two characteristic peaks, as presented in **Fig. 1b**, where one peak (*i.e.*, G-band) is located at ~1587 cm^{-1} and the other (*i.e.*, D-band) is centered at ~1332 cm^{-1}. The former is commonly attributed to the vibration of sp^2-bonded carbon atoms in a 2 D hexagonal lattice, that is, the stretching modes of C=C bonds of typical graphite. Note that the up-shifted peak relative to its position for perfect graphite is clearly observed, which indicates somewhat disorder in the resulting CDMMC material, due to the homogeneously doping of the heteroatoms of N and O.[36, 37] And the latter is associated to the vibrations of carbon atoms with dangling bonds in plane terminations of the disordered graphite, which is ascribed to the structural defects and disorders in carbon materials.[36, 37] The intensity ratio of "D-band" to "G-band", also known as the "*R*-value", reveals the amount of structurally ordered graphite crystallites in the carbonaceous materials, and reflects the graphitization degree of the carbon. Notably, the "*R*-value" of the as-obtained hierarchical CDMMC specimen is estimated as ~1.05, which should be responsible well for the desirable electronic conductivity (~23 S cm^{-1}) of the CDMMC product.

To further figure out the surface chemistry of the hierarchical CDMMC material, the intrinsic nature of C, O and N species in the CDMMC backbone was systematically investigated by the XPS technique. **Fig. 1(c-e)** depict the XPS data and corresponding fitted plots. The representative survey spectrum of C1s, as evidence in **Fig. 1c**, can be deconvoluted into the following four bands: C in rings (*i.e.*, C*-H) without N at 284.6 eV (C-I, ~22.1 at.%), C singly bound to O in phenol and ether (*i.e.*, C*-OH, or C*-O-*C) and C*-N groups at 286.1 eV (C-II, ~47.1 at.%), C sp^2 linked to N (*i.e.*, C*=N) and O (*i.e.*, C*=O, or O-C*-O) groups around at 287.8 eV (C-III, ~29.6 at.%) and C in carbonate groups and/or adsorbed CO_2 at 290.8 eV (C-IV, ~1.2 at.%).[38-40] In the region of N 1s core level spectrum (**Fig. 1d**), the chemical states of the N atom, with binding energies (BEs) of 400.1, 401.8 and 403.2 eV, can be identified as the N-pyrrolic/N-pyridonic (N-I, ~2.5 at.%), the N-quaternary (N-Q) (N-II, ~87.5 at.%)) and oxidized N-oxide species (N^+-O^-) (N-III, ~10.0 at.%), respectively, by using a Gaussian fitting method.[12, 15, 40, 41] As announced previsously,[42] the pseudo-

capacitive interactions just take place on negatively charged N-I, while the positive charger on N-II and N-III helps for electron transfer through the CDMMC material, which greatly favors for its improved electronic conductivity, and accounts well for the strong G-band in **Fig. 1b**. Three characteristic peaks at BEs of 531.3, 533.4 and 534.9 eV in the O 1s spectrum (**Fig. 1e**) can be related to the O in the quinine type group (*i.e.*, O*=C) (O-I, ~81.0 at.%), other O groups (*i.e.*, C-O*-H phenol and/or C-O*-C ether, O-II, ~5.3 at.%), and chemisorbed oxygen and/or water (O-III, ~13.7 at.%) bound to the hierarchical CDMMC surface,[12] of which only the "O*=C" group, *i.e.*, O-I, is considered to represent the pseudo-capacitive effect.[42, 43] The contributions of each species obtained by fitting the C 1s, N 1s, and O 1s core level spectra for the CDMMC are collected and listed in **Table 1**, as well as XPS peak positions and relative concentrations of each other. The atomic contents of C, O and N species are calculated quantitatively as ~80.5, ~15.5, and ~4.0 at.%, respectively, and their chemical formulas of N- and O-containing surface functional groups upon the CDMMC matrice are schematically show in **Fig. 2**. Additionally, the as-synthesized CDMMC product presents good wettability, as observed from the contact angle of ~36 ° (**Fig. S1**, Electronic Supporting Information, ESI†), which is reasonably attributable to the introduction of hydrophilic groups, that is, oxygen and nitrogen-based functional groups, on its surface. It will promote deep wetting by the electrolyte into the micro-scale particles, and make even more inner surfaces ion accessible for energy storage.

Fig. 3a, **b** gather representative FESEM images of the hierarchical CDMMC product. Apparently, the sample is morphologically monolithic with irregular particles of ~10 – 40 μm in size. TEM and HRTEM measurements were also carried out to further examine the microstructures of the as-synthesized CDMMC material more clearly. As can be seen from **Fig. 3(c-f)**, a structurally defective porous architecture with only local aromatic ordering and highly interconnected pores and channels in the nano-scaled and/or sub-nanometer range is clearly observed. To better understand the hierarchically porous structure and SSA parameters, we measured N_2 adsorption-desorption isotherms (**Fig. 4**) of the hierarchical CDMMC, and the corresponding porous properties of the

resultant CDMMC material are summarized in **Table 1**. As demonstrated in **Fig. 4a**, the N_2 adsorption-desorption isotherm is close to a combination form of type I and type IV according to the International Union of Pure and Applied Chemistry (IUPAC) classification, indicating the co-existence of micropores and mesopores formed in the product.[12, 15, 22, 24, 35, 44] In specific, the steep increase, that is, a sharp rise of N_2 uptake at relatively low pressure ($\leq$ 0.01 P/P_0) reveals the existence of rich micropores. The following slope at the medium relative pressure of 0.35 – 0.65 P/P_0 as well as the type H3 hysteresis loop, associated with capillary condensation taking place in mesopores, illustrates the presence of well-developed mesoporosity. The corresponding mesopore size distribution (**Fig. 4b**) calculated by the BJH method reveals the pore size is mainly between 2 – 4.5 nm and the PSD is quite narrow with a maximun located at ~2 nm. While there is relatively broad micropore distribution, estimated by the HK method, in the range of 0.4 – 1.7 nm with a sharp maximun centered at 0.68 nm (**Fig. 4c**). The BET SSA calculated from the adsoption branch reaches as high as ~1358 m^2 g^{-1}. The total pore volume is ~1.23 cm^3 g^{-1} determined from the N_2 adsorption amount at P/P_0 = 0.97, while the micropore volume is 0.56 cm^3 g^{-1} according to *t*-plot calculation. By determine the ratio of the micropore volume to total pore volume of the as-prepared CDMMC, 45.5% of the porosity thus comes from the micropores. And the average pore size of the hierarchical CDMMC sample is calculated as ~3.6 nm accordingly. On the basis of the analysis of N_2 sorption measurement, the CDMMC sample not only possesses large SSA but has well-developed porosity ranging from micro- to mesoscales. And the mesopores in the CDMMC sample are vital for furnising a smooth and convinient ion-transfer pathway, and thus enhance electrolyte accessibility to the microporous area for rapid charge storage.

It is also worthy of mentioning that the dimension of electrolyte ions is also of great significance to the efficient energy storage. The dimensional order of various ions of aqueous and/or organic electrolytes utilized in the work is presented as follows:[45-48]

$$OH^- < K^+ \approx H_3O^+ (3.62 – 4.2\ Å) < BF_4^- (4.6\ Å) < SO_4^{2-} (5.33\ Å) < TEA^+ (7.0\ Å)$$

Evidently, the micropore distribution observed here is basically larger and/or comparable to the size of hydrated ions in the applied KOH/H_2SO_4 electrolytes, and the ionic radii of TEA^+ and BF_4^- in PC, considering the solvation of ions in nonaqueous electrolyte. The good matching suitability of the dimension of electrolyte ions and pore size of eleltrode is therefore in great favor of effective energy storage, particularly at high rates.

3.2 Electrochemical evaluation.

It is owing to the presence of large SSA and moderate volume from the hierarchial micro-/mesopores, along with the rich N and O species in the carbon framework, that the as-prepared CDMMC material can be highly expected to perform as a high-performance electrode for advanced ECs. Nextly, we tested the hierarchical CDMMC material both in aqueous acidic (1 M H_2SO_4) and basic (6 M KOH) electrolytes by using three-electrode-cell layouts. To better understand the electrochemical process in these distinct electrolytes, CV and galvanostatic charge/discharge (GCD) curves were firstly performed to characterize the electrochemical properties of our CDMMC material in a potential window of 1.0 V (*vs.* SCE). **Fig. 5a** illustrates the typical CV curves of the CDMMC electrode at various sweeping rates ranged from 5 to 100 mV s^{-1} in KOH aqueous solution of 6 M. Apparently, the CDMMC sample exhibits representative capacitive behavior with rectangular-shaped voltammetry characteristics with respect to the zero-current line and a rapid current response on voltage reversal at each end potential, even at a high potential sweep rate of 100 mV s^{-1}, suggesting its excellent electric double-layer capacitive nature from -1.0 to 0.0 V (*vs.* SCE) in 6 M KOH. As a sharp contrast, the typical *E-I* response (**Fig. 5b**), from 0.0 to 1.0 V (*vs.* SCE) of the CDMMC electrode exhibits even larger electrochemical currents, revealing the enhanced capacitance of the CDMMC electrode in 1 M H_2SO_4 electrolyte. Of particular note, a distorted rectangular-like shape with extra appearance of prominent broad and overlapped humps is also evident in the CV curves (**Fig. 5b**) in 1 M H_2SO_4, which should originate from the combination of EDLC and Faradaic pseudo-capacitance related to the heteroatom functionalities of the CDMMC, rather than the single EDLC contribution in 6 M KOH. Furthermore, noticable deviation from "box-

like" shape is clearly demonstrated with the scan rate increasing up to high sweep rates (such as, 50, 80 and 100 mV s^{-1}), as seen in **Fig. 5b**, which further strongly confirms the pseudo-capacitive contribution from the surface redox reactions of the N- and O-functionalities in acidic system once again.[17, 41, 49] Furthermore, it is worthy to be noted that both of the electrochemically cathodic and anodic peak currents vary linearly with the sweeping rates (**Fig. S2**, ESI†). This data demonstrates that the hierarchical CDMMC electrode still possesses excellent rate behavior, although Faradaic reactions are involved in the electrochemical process of the CDMMC in H_2SO_4 electrolyte. And it is easy to concluded that the typical capacitive behavior observed here is also not diffusion controlled.[2, 50, 51]

To further evaluate the potential application of the as-obtained hierarchical CDMMC material as an attractive electrode for high-performance ECs application both in KOH and H_2SO_4 electrolytes, CP measurements over a large current range of 0.5 to 10 A g^{-1} were conducted systematically with three-electrode configuration. **Fig. 5c** plots the typical charging/discharging curves within the potential window from -0.1 to 0.0 V (*vs.* SCE) at various current densities as indicated in 6 M KOH, while **Fig. 5d** shows those for 1 M H_2SO_4 solution. Non-linear charge/discharge curves are obviously demonstrated in **Fig. 5d**, resulting from the electrochemical adsorption-desorption and redox reactions at the electrode/electrolyte interface in H_2SO_4 electrolyte, as aforementioned. In addition, the gravimetric SCs of the CDMMC electrode measured with the three-electrode configure are calculated from the CP plots in **Fig. 5c**, **d**, and the typical SCs in basic and acidic media as a function of discharge current density are collected in **Fig. 5e**, **f**, respectively. Accordingly, the mass SCs of the hierarchical CDMMC in 6 M KOH solution are estimated as ~363, ~236, ~191, ~180, ~169 and ~156 F g^{-1} at specific current rates of 0.5, 1.0, 2.0, 3.0, 5.0 and 10 A g^{-1}, respectively, as presented in **Fig. 5e**. In contrast, the electrode delivers much larger SCs of 460, 390, 332, 304, 269 and 218 F g^{-1} at specific current densities of 0.5, 1.0, 2.0, 3.0, 5.0 and 10 A g^{-1} in 1 M H_2SO_4 electrolyte (**Fig. 5f**), respectively. Therefore, the SC retentions of the CDMMC electrode retain as ~43% (6 M KOH) and ~47% (1 M H_2SO_4), respectively, when the current

density increases up to 10 from 0.5 A g^{-1}. It strongly suggests the good rate behavior of the CDMMC electrode in both the two electrolytes, benefiting from its enhanced electronic conductivity due to the typical nitrogen functionality, particularly the richness in bulk N of the CDMMC product.[3, 10-13, 15] The good electronic conductivity of the CDMMC can be further confirmed by small solution resistance (R_s) of ~0.41 Ohm (1 M H_2SO_4) and ~0.56 Ohm (6 M KOH) from the EIS analysis (**Fig. S3**, ESI†). More strikingly, the surface area normalized capacitances of the CDMMC, considering its BET SSA, are calculated as ~26.3 and ~33.4 μF cm^{-2} at a current density of 0.5 A g^{-1} in KOH and H_2SO_4 electrolytes, respectively, much higher than the theoretical EDLC capacitance of the carbonaceous materials (10 – 25 μF cm^{-2}),[4, 52] verifying its high electrochemical surface utilization both in acidic and basic aqueous electrolytes, thanks to its improved wettability (**Fig. S1**, ESI†) and proper hierarchical micro-/mesoporous feature (**Fig. 4**). All in all, the supercapacitive performance in acidic electrolyte (**Fig. 5f**) is presented even better than in basic electrolyte (**Fig. 5e**), as discussed above. Taking high nitrogen and oxygen contents into account, the larger SCs in H_2SO_4 electrolyte therefore should be rationally attributed to a more sensitive effect of the basic oxygenated and nitrogenated surface functional groups in 1 M H_2SO_4, which gives rise to extra pseudo-capacitive effects owing to sufficient Faradaic redox reactions in acidic medium (**Fig. 6**).[53-55] In common, because of the smaller size of K^+ and OH^-, compared to those of H^+ and SO_4^{2-}, as mentioned above, the double-layer capacitance contribution of electroadsorption to the overall capacitance in 6 M KOH should be more pronounced than that in 1 M H_2SO_4 electrolyte. Nevertheless, the overall SCs observed in 6 M KOH are much smaller than those in 1 M H_2SO_4 herein. This strongly confirms the significant attribution from the doped N and O atoms, and the resultant pseudo-capacitance once more. Thus, we take that as proof-of-principle for the importance of structurally incorporated N and O species for the enhancement of the supercapacitive performance in 1 M H_2SO_4. More importantly, from a comprehensive comparison of the SCs of the CDMMC electrode *versus* recently published high-performance heteroatom-rich carbons, all tested in a three-electrode systems (**Table S1,** ESI†), the CDMMC electrode obviously

exhibits comparable to and/or even higher SCs than those listed in **Table S1**, especically when considering an "apples to apples" comparison for those employing an electrochemically working window of 1.0 V (*vs.* SCE).

Electrochemical performance (**Fig. 7**) of the CDMMC-based symmetric ECs were also evaluated face-to-face by using two identical electrodes in acid and basic media within an electrochemical voltage range of 1.0 V (1 M H_2SO_4) and 0.9 V (6 M KOH), respectively. As evident in CV curves (**Fig. 7a**, **b**), the hierarchical CDMMC-based symmetric cells present quasi-retangular shape at a wide scanning rate span of 5 to 100 mV s^{-1}, suggesting the appealing electrochemical capacitance of the symmetric device both in H_2SO_4 and KOH electrolytes. Strikingly, the higher electrochemical current response and larger intergrated area under the *I-E* curve are observed in **Fig. 7a**, compared to those in KOH (**Fig. 7b**), which further reveals superior energy-storage ability of the EC in the acidic medium, owing to intriguing peseudo-capacitive contribution in such system. **Fig. 7c**, **d** demonstrate the typical GCD plots at various current densities ranged from 0.5 to 5 A g^{-1}, considering both the mass of the the two electrodes, in 1 M H_2SO_4 and 6 M KOH aqueous solutions. Expressly, the longer charging and/or discharging time of the CDMMC-based EC are found in the acidic electrolyte, revealing the enhanced SCs in the electrolyte, compared to those in basic medium at the same rate. Furthermore, the higher coulombic efficiency (CE), in contrast with that in 6 M KOH, is also presented for the CDMMC-based EC in aqueous H_2SO_4 solution, as shown in **Fig. 7e**. Impressively, the symmetric EC delivers a high SC of ~53 F g^{-1} at 0.5 A g^{-1}, and even ~33 F g^{-1} at a large current loading of 5 A g^{-1} in H_2SO_4 solution, much higher than those in KOH solution at the same rates, as seen in **Fig. 7f**. All in all, the aforementioned data strongly confirms even better electrochemical capacitance of the symmetric EC in acidic electrolyte.

As well known before, the use of organic electrolytes is in high demand because of their large working potential window for advanced ECs with large SED.[45, 56] In common, much higher energy densities, compared to those of the aqueous electrolytes (~1.0 V, due to the thermodynamic

electrochemical window of water),[45] would be obtained from the ECs with organic electrolytes, as the energy density is equal to the square of the electrochemically working potential range. Accordingly, the electrochemical performance of a fully assembled CDMMC-based asymmetric EC is further evaluated tentatively in a voltage range of 2.5 V with an organic electrolyte of 1 M $TEABF_4$/PC. **Fig. 8a** presents the representative CV curves of the symmetric EC with 1 M $TEABF_4$/PC electrolyte. Clearly, at a relative low scan rates (such as, 5, 10, 20 mV s^{-1}), the CV curves are nealy rectangular-like with positive sweeps nearly mirror-image symmetric to their corresponding counterparts on the negative sweeps with respect to the zero-current line. As the scan rate increases up to 100 mV s^{-1}, the current subsequently increases while the CV shape changes little and rapid current response on voltage reversal occurs at end potential, strongly demonstrating rapid charge-discharge kinetics of the symmetric device with 1 M $TEABF_4$/PC. As seen in **Fig. 8b**, linear GCD curves are apparently presented, revealing the desirable electrochemical behavior of the symmetric EC in such organic electrolyte. Attractively, the unique EC exhibits remarkable SCs of ~20.6, ~20.2, ~18.0, ~15.1, ~11.8, ~11.1 and ~11.5 F g^{-1} at 0.1, 0.5, 1, 2, 3, 4 and 5 A g^{-1}, respectively, in 1 M $TEABF_4$/PC, which shows that ~56% of the capacitance is still maintained when the charge-discharge current increases from 0.1 to 5 A g^{-1}, highlighting its desirable rate property. However, the SCs delivered by the CDMMC-based EC with the organic electrolyte are notably smaller than those with aqueous solutions. The reasons for such phenomnon should be rationally ascribed to the modest compatibility between the electroactive CDMMC material and $TEABF_4$/PC electrolyte, which prevents the electrolyte from adquately accessing the external surface and inner volume of the CDMMC sample, resulting in just limited outer-surface accessibility. Also as examined from the EIS of the symmetric EC with 1 M $TEABF_4$/PC (**Fig. S4**, ESI†), the larger equivalent series resistance (~2.1 Ohm) and charge-transfer resistance (~18.6 Ohm) are presented, which should be responsible well for the smaller SCs observed in such organic electrolyte. Additionally, the cyclability of the symmetric EC with 1 M $TEABF_4$/PC electrolyte is one of the significant aspects for its practical application. **Fig. 8d** illustrates the long-term

electrochemical stability of the symmtric device investigated by using CP measurement at a current rate of 0.5 A g^{-1} within a potential window of 0.0 – 2.5 V. Obviously, the SC even maintains at ~92% of the initial value over 5000 continuous cycles, displaying excellent stability of the CDMMC-based EC with 1 M $TEABF_4$/PC electrolyte. Moreover, the CE of the unique EC basically keeps more than 97% during the continuous charge-discharge cycles, as shown in **Fig. 8d**. Electrochemical data recorded here strongly highlights the capability of the hierarchical CDMMC-based symmetric EC to meet the requirements of good electrochemical stability with high reversibility during the long-term cycling under a high-power operation, which is significant merit for the practical ECs.

Ragone plots in organic, aqueous acidic and basic electrolytes are further depicted in **Fig. 9**. The highest SED of ~17.9 Wh kg^{-1} in a aprotic electrolyte of 1 M $TEABF_4$/PC has been obtained for the symmetric EC at the SPD of 125 W kg^{-1}, owing to its larger electrochemically working window of 2.5 V (**Fig. 8a**). Also notedly, the SED observed in such organic electrolyte is comparable to, and even higher than some other asymmetric systems, such as, activated carbon (AC)/MnO_2 (~17 Wh kg^{-1}),[57] $Li_4Ti_5O_4$/AC (~18 Wh kg^{-1}),[58] *etc*. Furthermore, the SED is still obtained by the EC with 1 M $TEABF_4$/PC as large as ~10.1 Wh kg^{-1} at a high SPD of 6250 W kg^{-1}. In a sharp contrast, the symmetric device only delivers modest SED of ~7.3 and ~3.4 Wh kg^{-1} in 1 M H_2SO_4 and 6 M KOH electrolytes, respectively, which should be mainly attributed to the narrow potential ranges (1.0 V for 1 M H_2SO_4 and 0.9 V for 6 M KOH) in aqueous solutions (**Fig. 7a**, **b**). In addition, the symmetric device with the $TEABF_4$/PC electrolyte can efficiently power a 3 mm-diameter blue round lighting emitting diode (LED) indicator for more than 60 s, as presented in the inset in **Fig. 9d**.

4. Conclusions

In conclusion, we herein put forward a facile yet scalable synthesis of hierarchical N- and O-functionalized carbon material with nanoscale to mesoscale porous structures by using disposable and renewable cashmere as the raw material. The resultant hierarchical CDMMC was endowed with

disirable SSA (1358 m^2 g^{-1}), hierarchical porosity (1.23 cm^3 g^{-1}) with high microporosity of 45.5%, and high content of heteroatom functionalities (N of ~4 at.% and O of ~15.5 at.%). It was the striking synergetic effect of these structural and compositional advantages that delivered exquisite electrochemical performance to the as-fabricated hierarchical CDMMC material both in aqueous H_2SO_4 and KOH electrolytes. Remarkably, even larger electrochemical capacitance was observed in 1 M H_2SO_4, which could be attributed to the micro-/mesoporosity coupled with high effective surface area and heteroatom (N, O) doping effects. In addition, larger SED of ~17.9 Wh kg^{-1} was obtained for the CDMMC-based symmetric supercapacitor with an electrochemical window of 2.5 V in 1 M $TEABF_4$/PC, compared to those in aqueous electrolytes. More significantly, the strategy proposed here provides an excellent sample to make best of the cost-effective yet abundant resources endowed by nature to fabricate sustainable high-performance electrode materials for next-generation ECs, thus opening new avenues to set up an economical platform to synthesize advanced porous heteroatom-functionalized carbons available in a large spectrum of practical applications, including Li-ion batteries, biosensor, catalysis, and so on.

Acknowledgements

The authors are grateful to the financial supports from the National Natural Science Foundation of China (no. 51202004), Anhui Province Funds for Distinguished Young Scientists, the Natural Science Foundation of Anhui Province (no. KJ2013A051), the Foundation for Young Talents in College of Anhui Province, and the Opening Project of CAS Key Laboratory of Materials for Energy Conversion (no. 2014001).

† Electronic Supplementary Information (ESI) available: Contact angle of the product, electrochemical performance of the samples. See DOI: 10.1039/b000000x/

Notes and References

[1] P. Simon and Y. Gogotsi, *Nat. Mater.*, 2008, **7**, 845-854.

[2] T. Brezesinski, J. Wang, S.H. Tolbert and B. Dunn, *Nat. Mater.*, 2010, **9**, 146-151.

[3] F. Béguin, K. Szostak, G. Lota and E. Frackowiak, *Adv. Mater.*, 2005, **17**, 2380-2384.

[4] B. E. Conway, Electrochemical supercapacitors: Scientific Fundamentals and Technological Applications (Kluwer, 1999).

[5] Y. G. Wang, Z. S. Hong, M. D. Wei and Y. Y. Xia, *Adv. Funct. Mater.*, 2012, **22**, 5185-5193.

[6] C. Z. Yuan, L. Yang, L. R. Hou, J. Y. Li, Y. X. Sun, X. G. Zhang, L. F. Shen, X. J. Lu, S. L. Xiong and X. W. Lou, *Adv. Funct. Mater.*, 2012, **22,** 2560-2566.

[7] L. R. Hou, C. Z. Yuan, D. K. Li, L. Yang, L. F. Shen, F. Zhang and X. G. Zhang, *Electrochim. Acta*, 2011, **56**, 7454-7459.

[8] C. Z. Yuan, L. H. Zhang, L. R. Hou, J. D. Lin and G. Pang, *RSC Ad*v., 2014, **4**, 24773-2476.

[9] C. Z. Yuan, B. Gao, L. F. Shen, S. D. Yang, L. Hao, X. J. Lu, F. Zhang, L. J. Zhang and X. G. Zhang, *Nanoscale*, 2011, **3**, 529-545.

[10] J. P. Paraknowitsch and A. Thomas, *Energy Environ. Sci.*, 2013, **6**, 2839-2855.

[11] B. K. Guo, X. G. Sun, G. M. Veith, Z. H. Bi, S. M. Mahurin, C. Liao, C. Bridges, M. P. Paranthaman and S. Dai, *Adv. Energy Mater.*, 2013, **3**, 708-712.

[12] W. J. Qia, F. X. Sun, Y. H. Xu, L. H. Qiu, C. H. Liu, S. D. Wang and F. Yan, *Energy Environ. Sci.*, 2014, **7**, 379-386.

[13] H. M. Sun, L. Y. Cao and L. H. Lu, *Energy Environ. Sci.*, 2012, **5**, 6206-6213.

[14] L. Borchardt, M. Oschatz and S. Kaskel, *Mater. Horiz.*, 2014, **1**, 157-168.

[15] W. R. Li, D. H. Chen, Z. Li, Y. F. Shi, Y. Wan, J. J. Huang, J. J. Yang, D. Y. Zhao and Z. Y. Jiang, *Electrochem. Commun.*, 2007, **9**, 569-573.

[16] J. Chmiola, G. Yushin, Y. Gogotsi, C. Portet, P. Simon and P. L. Taberna, *Science*, 2006, **313**, 1760-1763.

[17] L. Z. Fan, S. Y. Qiao, W. L. Song, M. Wu, X. B. He and X. H. Qu, *Electrochim. Acta*, 2013, **105**, 299-304.

[18] D. Hulicova-Jurcakova, A. M. Puziy, O. I. Poddubnaya, F. Suárez-García, J. M. D. Tascón and G. Q. Lu, *J. Am. Chem. Soc.*, 2009, **131**, 5026-5027.

[19] L. R. Hou, L. Lian, D. K. Li, G. Pang, J. F. Li, X. G. Zhang, S. L. Xiong and C. Z. Yuan, *Carbon*, 2013, **64**, 141-149.

[20] B. Xu, S. Hou, G. P. Cao, F. Wu and Y. S. Yang, *J. Mater. Chem.*, 2012, **22**, 19088-19093.

[21] M. Biswal, A. Banerjee, M. Deo and S. Ogale, *Energy Environ. Sci.*, 2013, **6**, 1249-1259.

[22] H. J. Liu, Y. L. Cao, F. Wang, W. D. Zhang and Y. Q. Huang, *Electroanal.*, 2014, **26**, 1831-1839.

[23] W. T. Huang, H. Zhang, Y. Q. Huang, W. K. Wang and S. C. Wei, *Carbon*, 2011, **49**, 838-843.

[24] H. J. Liu, Y. L. Cao, F. Wang and Y. Q. Huang, *ACS Appl. Mater. Interfaces* 2014, **2**, 819-825.

[25] W. X. Chen, H. Zhang, Y. Q. Huang and W. K. Wang, *J. Mater. Chem.*, 2010, **20**, 4773-4775.

[26] V. Subramanian, C. Luo, A. M. Stephan, K. S. Nahm, S. Thomas and B. Q. Wei, *J. Phys. Chem. C*, 2007, **111**, 7527-7531.

[27] X. J. He, P. H. Ling, M. X. Yu, X. T. Wang, X. Y. Zhang and M. D. Zheng, *Electrochim. Acta*, 2013, **105**, 635-641.

[28] Y. W. Ma, J. Zhao, L. R. Zhang, Y. Zhao, Q. L. Fan, X. A. Li, Z. Hu and W. Huang, *Carbon*, 2011, **49**, 5292-5297.

[29] H. Jin, X. M. Wang, Z. R. Gu, J. D. Hoefelmeyer, K. Muthukumarappan, J. Julson, *RSC Adv.*, 2014, **4**, 14136-14142.

[30] X. L. Gao, W. Xing, J. Zhou, G. Q. Wang, S. P. Zhuo, Z. Liu, Q. Z. Xue and Z. F. Yan, *Electrochim. Acta*, 2014, **133**, 459-466.

[31] C. Z. Yuan, L. Chen, B. Gao, L. H. Su and X. G. Zhang, *J. Mater. Chem.*, 2009, **19**, 246-252.

[32] Y. G. Wang, Z. D. Wang and Y. Y. Xia, *Electrochim. Acta*, 2005, **5**, 5641.

[33] C. Largeot, C. Portet, J. Chniola, P. L. Taberna, Y. Gogotsi and P. Simon, *J. Am. Chem. Soc.*, 2008, **130**, 2730.

[34] J. C. Wang and S. Kaskel, *J. Mater. Chem.*, 2012, **22**, 23710-23725.

[35] Z. Li, Z. W. Xu, H. L. Wang, J. Ding, B. Zahiri, C. M. B. Holt, X. H. Tan and D. Mitlin, *Energy Environ. Sci.*, 2014, **7**, 1708-1718.

[36] S. Mentus, G. Ćirić-Marjanović, M. Trchová and J. Stejskal, *Nanotechnology*, 2009, **20**, 245601.

[37] A. Janošević, I. Pašti, N. Gavrilov, S. Mentus, G. Ćirić-Marjanović, J. Krstić and J. Stejskal, *Synth. Met.*, 2011, **161**, 2179-2184.

[38] Z. R. Yue, K. R. Benak, J. W. Wang, C. L. Mangun and J. Economy, *J. Mater. Chem.*, 2005, **15**, 3142-3148.

[39] Y. Xie and P. M. A. Sherwood, *Chem. Mater.*, 1990, **2**, 293-299.

[40] Z. H. Wang, L. Qie, L. X. Yuan, W. X. Zhang, X. L. Hu and Y. H. Huang, *Carbon*, 2013, **55**, 328-334.

[41] A. B. Fuertes, G. A. Ferrero and M. Sevilla, *J. Mater. Chem. A*, 2014, **2**, 14439-14448.

[42] D. Hulicova-Jurcakova, M. Seredych, G. Q. Lu and T. J. Bandosz, *Adv. Funct. Mater.*, 2009, **19**, 438-447.

[43] H. A. Andreas amd B. E. Conway, *Electrochim. Acta*, 2006, **51**, 6510-6520.

[44] I. Cabasso, S. D. Li, X. W. Wang and Y. X. Yuan, *RSC Adv.*, 2012, **2**, 4079-4091.

[45] D. Hulicova, M. Kodama and H. Hatori, *Chem. Mater.*, 2006, **18**, 2318-2326.

[46] L. Eliad, G. Salitra, A. Soffer and D. Aurbach, *J. Phys. Chem. B*, 2001, **105**, 6880-6887.

[47] M. Endo, T. Maeda, T. Takeda, Y. J. Kim, K. Koshiba, H. Hara and M. S. Dresselhaus, *J. Electrochem. Soc.*, 2001, **148**, A910-A914.

[48] M. Ue, *J. Electrochem. Soc.*, 1994, **141**, 3336-3342.

[49] F. Béguin, E. Raymundo-piñero and E. Frackowiak, Carbons for electrochemical energy storage and conversion systems, CRC Press, 2010; pp: 329-375.

[50] A. J. Bard and L. R. Faulkner, Electrochemical methods fundamentals and applications, 2nd ed., John Wiley, Inc, New York 2001; Ch. 6, P: 233, 235.

[51] C. Z. Yuan, J. Y. Li, L. R. Hou, J. D. Lin, X. G. Zhang and S. L. Xiong, *J. Mater. Chem. A*, 2013, **1**, 11145-11151.

[52] H. Jiang, P. S. Lee and C. Li, *Energy Environ. Sci.*, 2013, **6**, 41-53.

[53] C. M. Chen, Q. Zhang, X. C. Zhao, B. S. Zhang, Q. Q. Kong, M. G. Yang, Q. H. Yang, M. Z. Wang, Y. G. Yang, R. Schlögl and D. S. Su, *J. Mater. Chem.*, 2012, **22**, 14076.

[54] Z. F. Zhou, Z. H. Zhang, H. R. Peng, Y. Qin, G. C. Li and K. Z. Chen, *RSC Adv.*, 2014, **4**, 5524.

[55] D. W. Wang, F. Li, L. C. Yin, X. Lu, Z. G. Chen, I. R. Gentle, G. Q. Lu and H. M. Cheng, *Chem. Eur. J.*, 2012, **18**, 5345.

[56] W. R. Li, D. H. Chen, Z. Li, Y. F. Shi, Y. Wan, G. Wang, Z. Y. Jiang and D. Y. Zhao, *Carbon*, 2007, **45**, 1757-1763.

[57] Q. T. Qu, P. Zhang, B. Wang, Y. H. Chen, S. Tian, Y. P. Wu and R. Holze, *J. Phys. Chem. C*, 2009, **113**, 14020-14027.

[58] P. Simon and A. Burke, *J. Electrochem. Soc. Interface*, 2008, **17**, 38-43.

Table , Figures and Captions

Table 1. XPS peak positions, relative contents of C, O and N species, and pore texture parameters in the resultant hierarchical CDMMC product

C species (80.5 at.%)	Peak position (eV)	at.%	Texture parameters	
C-I	284.6	22.1	Specific surface area	
C-II	286.1	47.1	(m^2 g^{-1})	1378
C-III	287.5	29.6		
C-IV	290.8	1.2		
O species (15.5 at.%)			Average pore size	2.8
			(nm)	
O-I	531.3	81.0		
O-II	533.3	5.3		
O-III	534.9	13.7		
			Total pore volume	1.23
N species (4.0 at.%)			(cm^3 g^{-1})	
N-I	400.2	2.5		
N-II	401.5	87.5	Micropore volume	0.56
N-III	403.2	10.0	(cm^3 g^{-1})	

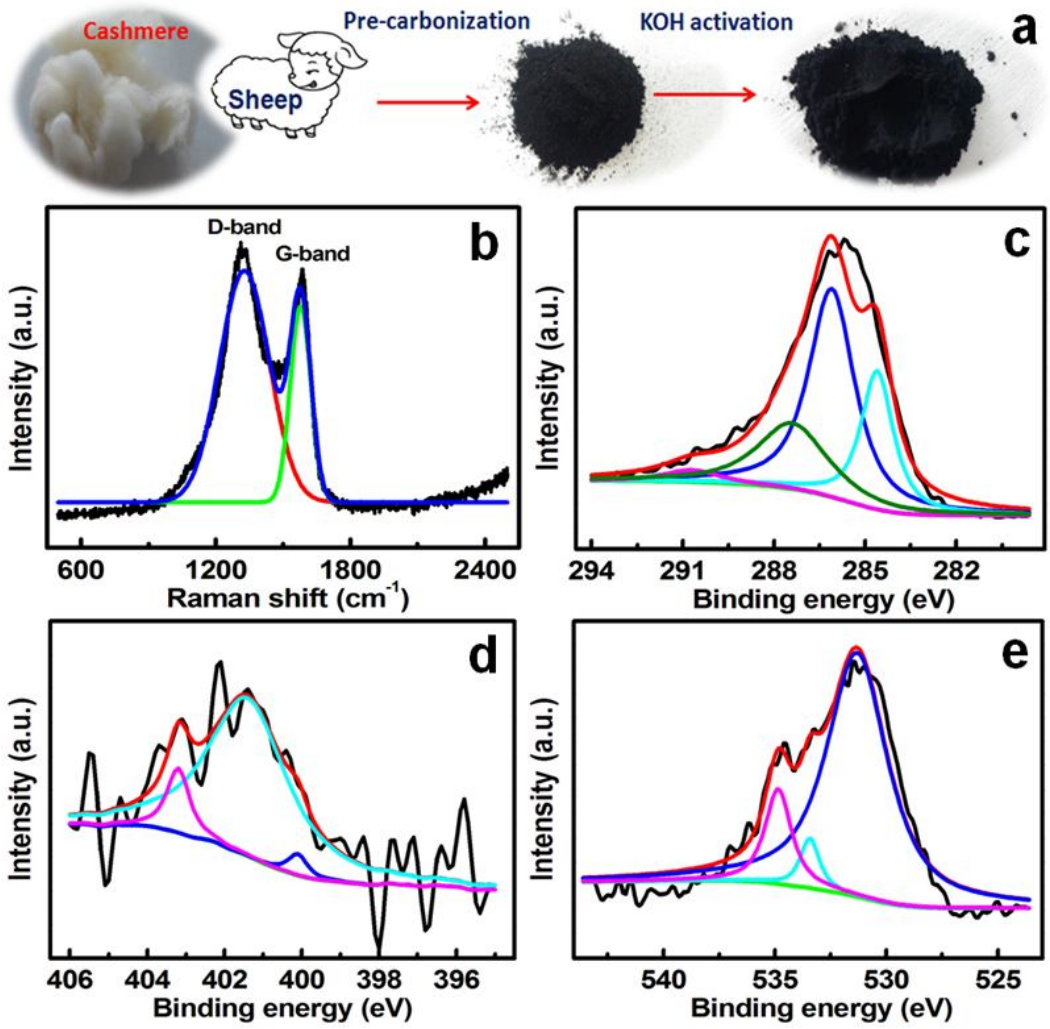

Fig. 1. (a) Schematic diagram for the fabrication of hierarchical CDMMC material; (b) Raman spectrum and fitted data, and High-resolution XPS spectra and fitted data of C 1s (c), N 1s (d) and O 1s (e) for the resulting CDMMC product

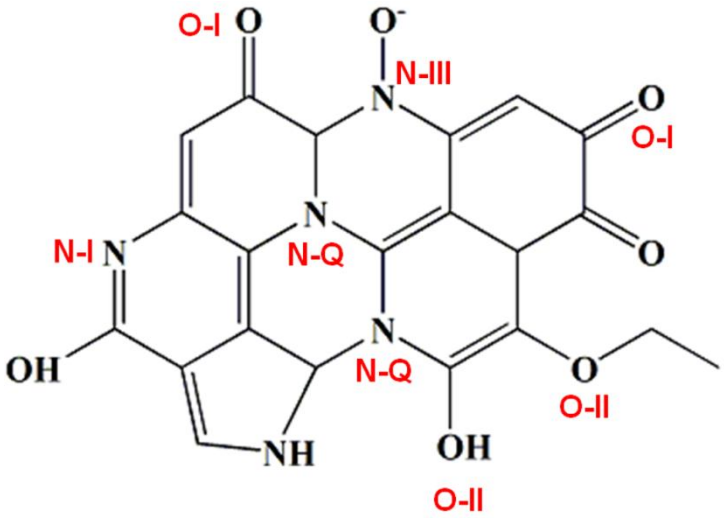

Fig. 2. Schematic models of N- and O-containing surface functional groups on the CDMMC sample

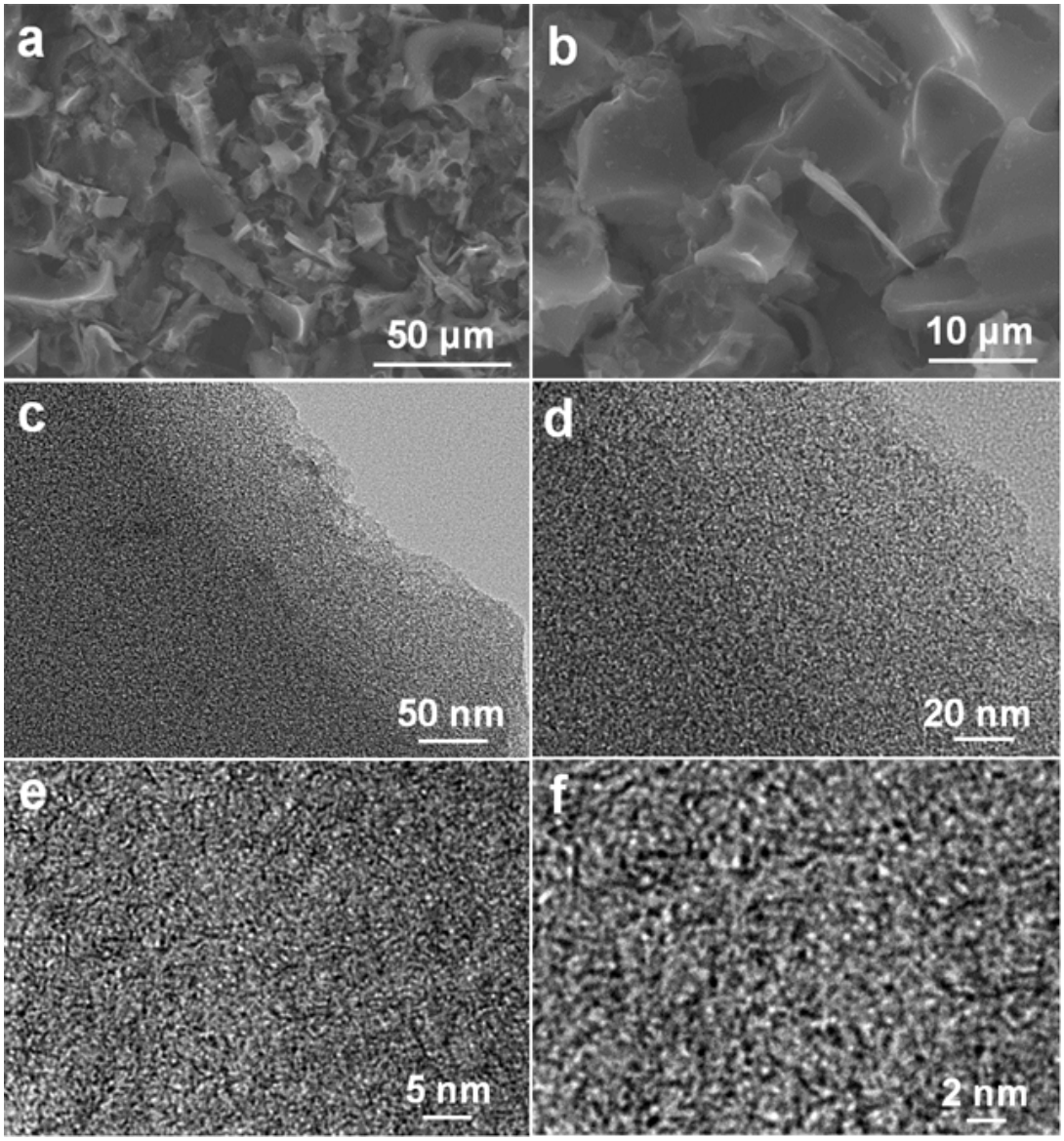

Fig. 3. (a, b) FESEM, (c, d) TEM and (e, f) HRTEM images of the as-obtained hierarchical CDMMC product

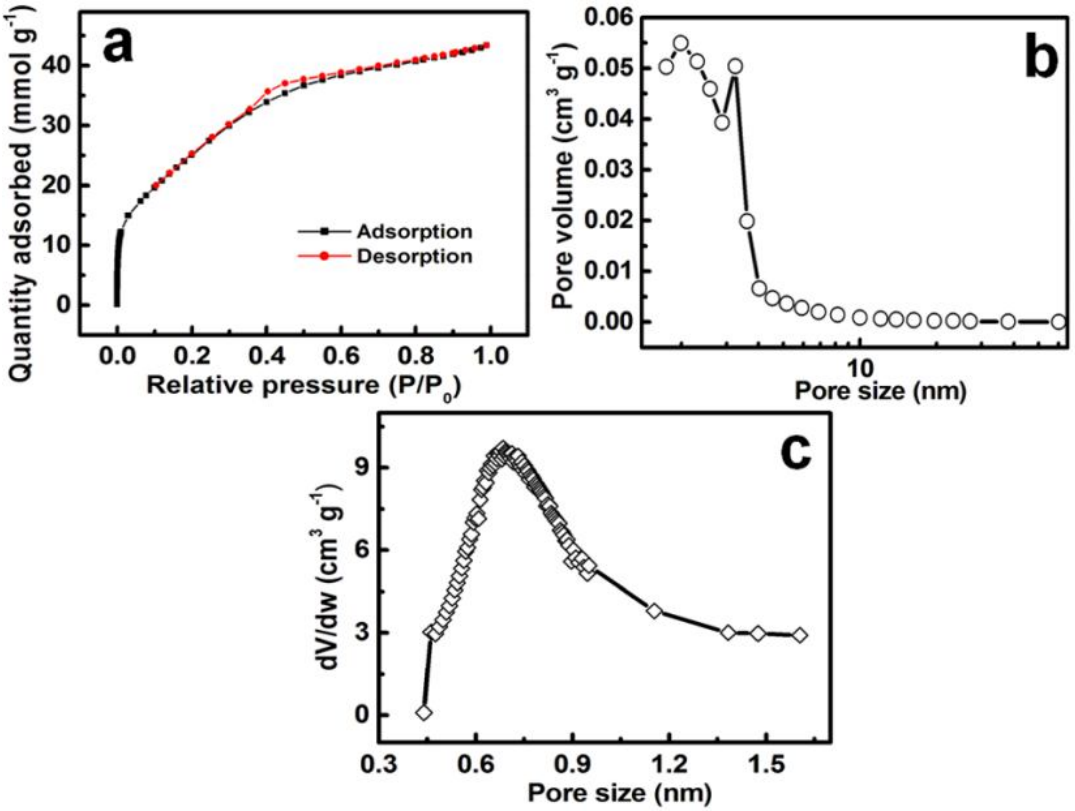

Fig. 4. (a) N_2 adsorption-desorption isotherm, and PSDs of (b) the mesopores and (c) micropores for the resultant hierarchical CDMMC material

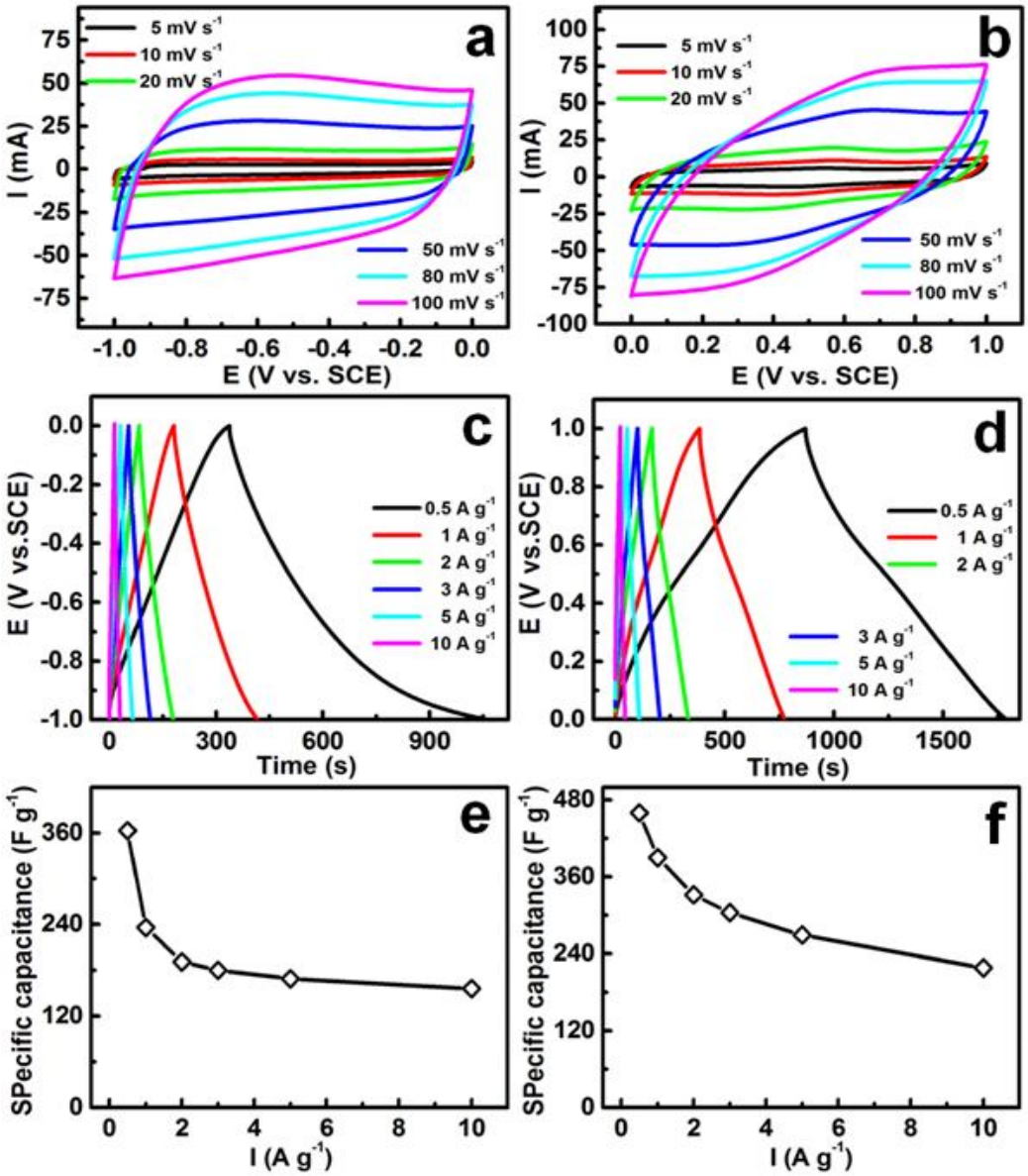

Fig. 5. Electrochemical evaluation of the CDMMC electrode in (a, c, e) 6 M KOH and (b, d, f) 1 M H_2SO_4 electrolyte: (a, b) CV curves with the scanning rate ranged from 5 to 100 mV s^{-1}; (c, d) GCD profiles at various current densities as indicated, and (e, f) the corresponding SCs as a function of current density.

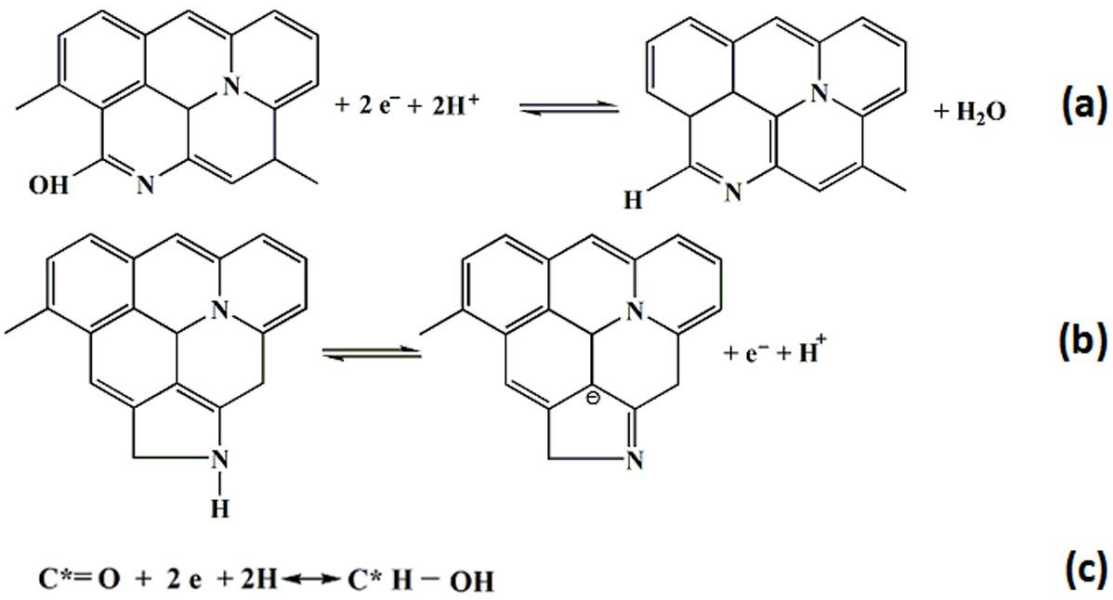

Fig. 6. Possible Faradaic charge transfer reactions involving: (a) pyridonic and (b) pyrrolic nitrogen groups, and (c) the oxygen doubly bound to the CDMMC in H_2SO_4 electrolyte

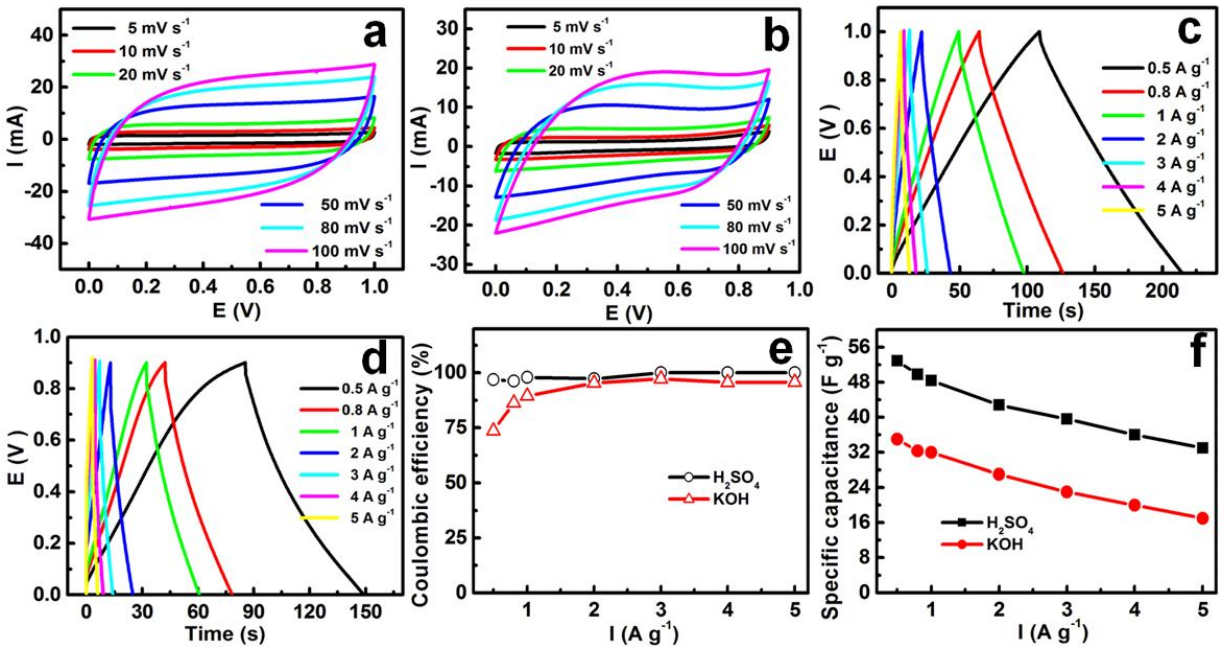

Fig. 7. (a, b) CV curves; (c, d) constant current charge-discharge voltage profiles for the hierarchical CDMMC-based symmetric ECs in (a, c) 1 M H_2SO_4 and (b, d) 6 M KOH electrolytes. (e) Corresponding CEs and (f) the SCs as a function of current density in different aqueous electrolytes as indicated

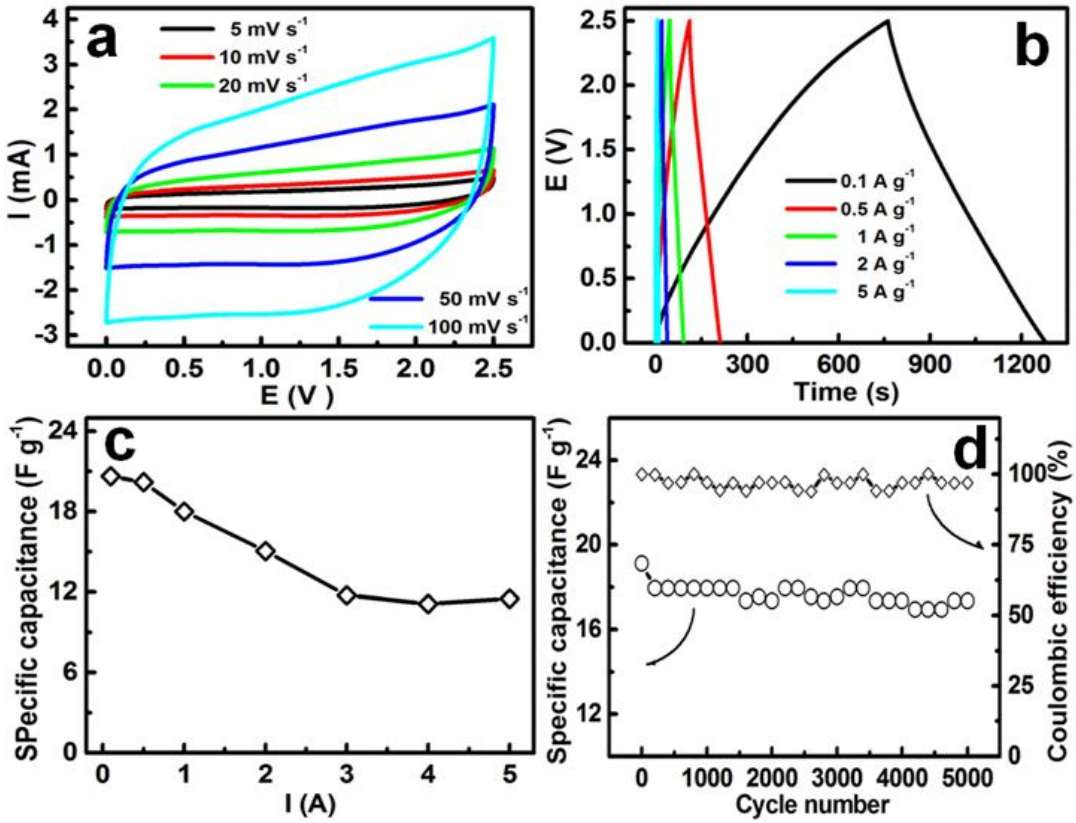

Fig. 8. Electrochemical evaluation of the hierarchical CDMMC-based symmetric EC with 1 M $TEABF_4$/PC electrolyte: (a) CV curves; (b) constant current charge-discharge profiles, and (c) the corresponding SCs as a function of current density; and (d) cycling performance and CE at a current density of 0.5 A g^{-1}

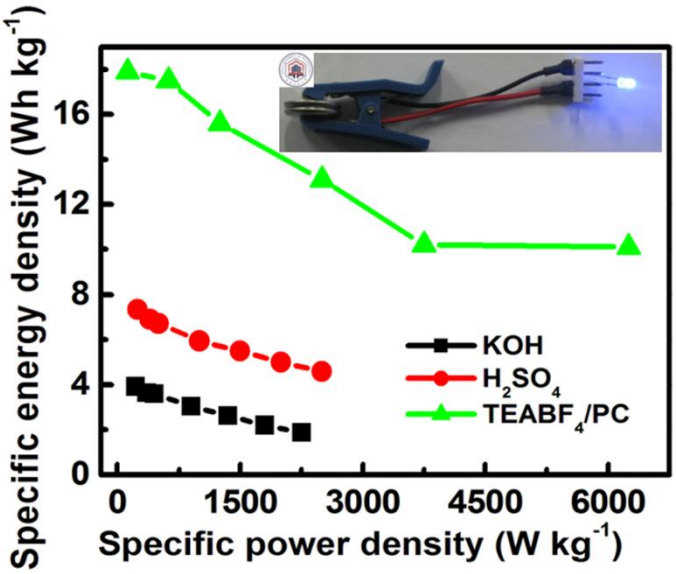

Fig. 9. Ragone plots of the hierarchical CDMMC-based symmetric ECs with different electrolytes as indicated. The inset for the optical image showing that a LED is powered by the symmetric device with 1 M $TEABF_4$/PC as the electrolyte

The Table of Contents entry

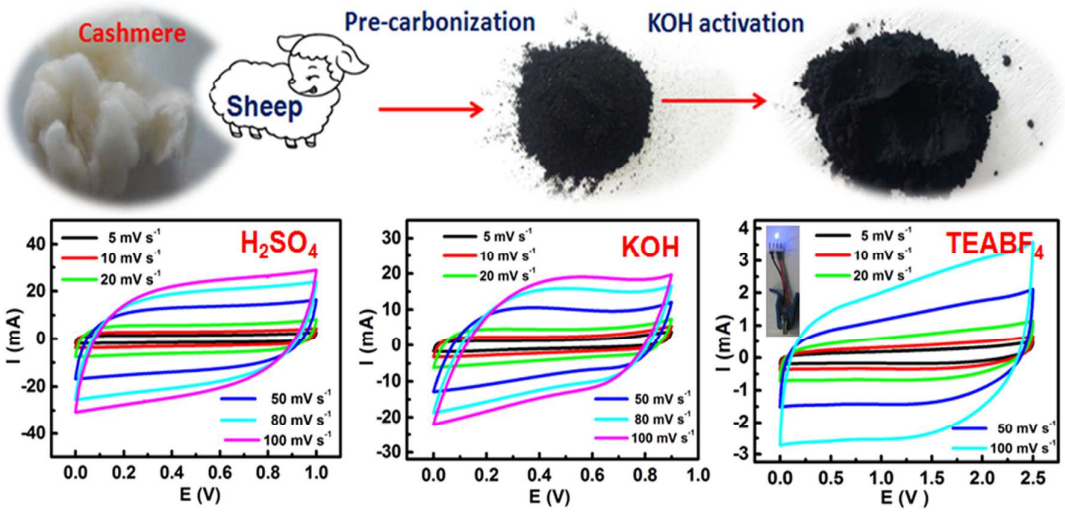

Hierarchical cashmere-derived micro-/mesoporous carbon, as competitive cost-effective material for advanced electrochemical capacitors, delivered excellent electrochemical capacitance at high rates

Supporting Information

Hierarchical micro-/mesoporous N- and O-enriched carbon derived from disposable cashmere: A competitive cost-effective material for high performance electrochemical capacitors

Lu Zhou [a], *Siqi Zhu* [a], *Hui Cao* [a], *Linrui Hou* [a] *and Changzhou Yuan* *[a, b]

[a] *School of Materials Science & Engineering, Anhui University of Technology, Ma'anshan, 243002, P.R. China*

E-mail: ayuancz@163.com

[b] *Chinese Academy of Science (CAS) Key Laboratory of Materials for Energy Conversion, Hefei, 230026, P.R. China*

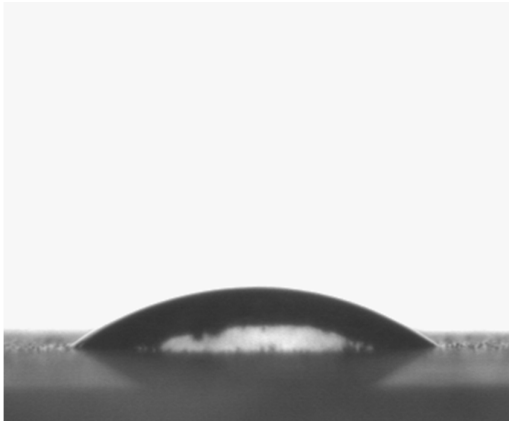

Fig. S1. Contact angle of the hierarchical CDMMC sample

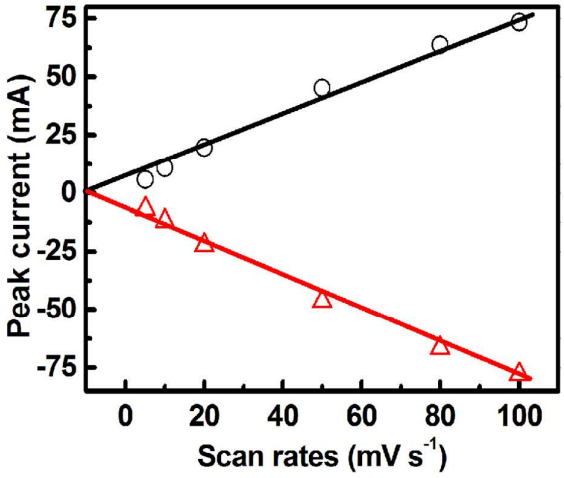

Fig. S2. Relationship between electrochemically cathodic and anodic redox peak currents and the sweep rate of the hierarchical CDMMC electrode in 1 M H_2SO_4 electrolyte

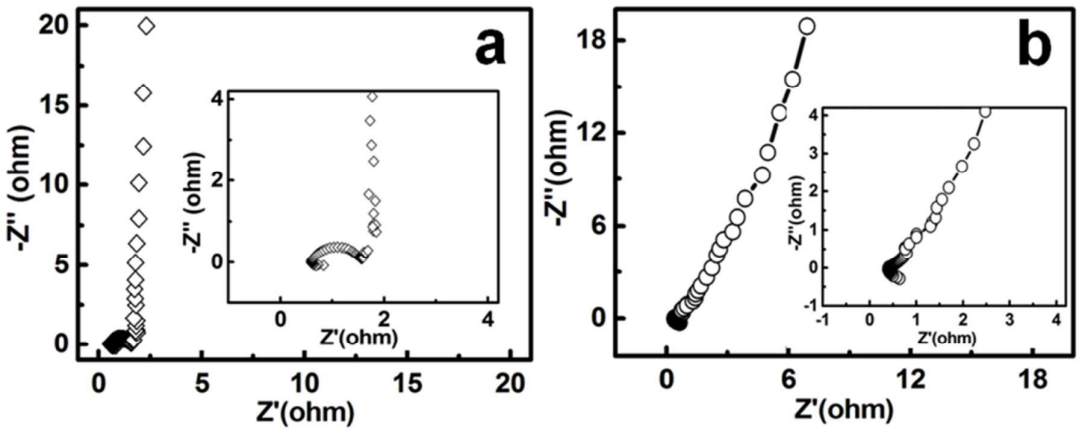

Fig. S3. EIS spectra of the CDMMC electrode in three-electrode configurations with (a) 6 M KOH and (b) 1 M H_2SO_4 solutions. The insets in (a, b) for the corresponding high-frequency regions of the EIS spectra, respectively

In general, the intersection of the plots at the X-axis represents solution resistance (R_s), which is associated with the following three items: the resistance of the aqueous solution, the intrinsic resistance of the electroactive material itself, and the contact resistance at the interface between electroactive material and current collector. As observed in **Fig. S3a**, **b**, the values for the R_s in the 6 M KOH and 1 M H_2SO_4 are observed as ~0.56 Ohm and 0.41 Ohm, respectively.

Table S1. SCs of the CDMMC *vs.* recently published heteroatom-rich carbons all tested in three-electrode configurations with different electrolytes

Carbon type	SCs (F g^{-1})/ discharge current density (A g^{-1})	electrolyte	electrochemical window (V)	Ref.
CDMMC	363/0.5	KOH	1.0	This work
CDMMC	460/0.5	H_2SO_4	1.0	This work
Porous N-doped CNT	220/0.5	KOH	1.0	[1]
Functionalized carbon	319/0.5	KOH	1.0	[2]
Hair-derived carbon	340/2.0	KOH	1.0	[3]
Nitrogen-doped graphene	280/<1.0	KOH	0.8	[4]
Leaves derived carbon	400/0.5	KOH	1.0	[5]
Partially reduced GO	347/0.2	H_2SO_4	1.0	[6]
Graphene-CNT architecture	326	H_2SO_4	1.0	[7]
Bacteria promoted carbon	327/1.0	H_2SO_4	1.0	[8]
N-containing HTC	300/0.2	H_2SO_4	1.0	[9]
Zeolite template carbon	340/0.1	H_2SO_4	1.2	[10]
PANI derived carbon	239/0.5	H_2SO_4	1.0	[11]
Rice husk	243/0.05	KOH	1.0	[12]

[1] G. Y. Xu, B. Ding, P. Nie, L. F. Shen, J. Wang, X. G. Zhang, *Chem. Eur. J.* **2013**, 19, 12306.

[2] L. Qie, W. Chen, H. Xu, X. Xiong, Y. Jiang, F. Zou, X. Hu, Y. Xin, Z. Zhang, Y. Huang, *Energy Environ. Sci.* **2013**, 6, 2497

[3] W. J. Qian, F. X. Sun, Y. H. Xun, L. H. Qiu, C. H. Liu, S. D. Wang, F. Yan, *Energy Environ. Sci.* **2014**, 7, 379.

[4] H. M. Jeong, J. W. Lee, W. H. Shin, Y. J. Choi, H. J. Shin, J. K. Kang, J. W. Choi, *Nano Lett.* **2011**, 11, 2472.

[5] M. Biswal, A. Banerjee, M. Deo, S. Ogale, *Energy Environ. Sci.* **2013**, 6, 1249.

[6] Y. Chen, X. O. Zhang, D. C. Zhang, P. Yu, Y. W. Ma, *Carbon* **2011**, 49, 573.

[7] S. Y. Yang, K. H. Chang, H. W. Tien, Y. F. Lee, S. M. Li, Y. S. Wang, J. Y. Wang, C. C. M. Ma, C. C. Hu, *J. Mater. Chem.* **2011**, 21, 2374.

[8] H. Sun, L. Cao, L. Lu, *Energy Environ. Sci.* **2012**, 5, 6206.

[9] L. Zhao, L. Z. Fan, M. Q. Zhou, H. Guan, S. Y. Qiao, M. Antonietti, M. M. Titirici, *Adv. Mater.* **2010**, 22, 5202.

[10] C. O. Ania, V. Khomenko, E. Raymundo-Pinero, J. B. Parra, F. Beguin, *Adv. Funct. Mater.* **2007**, 17, 1828.

[11] T. Bordjiba, M. Mohamedi, L. H. Dao, *Adv. Mater.* **2008**, 20, 815.

[12] X. J. He, P. H. Ling, M. X. Yu, X. T. Wang, X. Y. Zhang, M. D. Zheng, *Electrochim. Acta* **2013**, 105, 635.

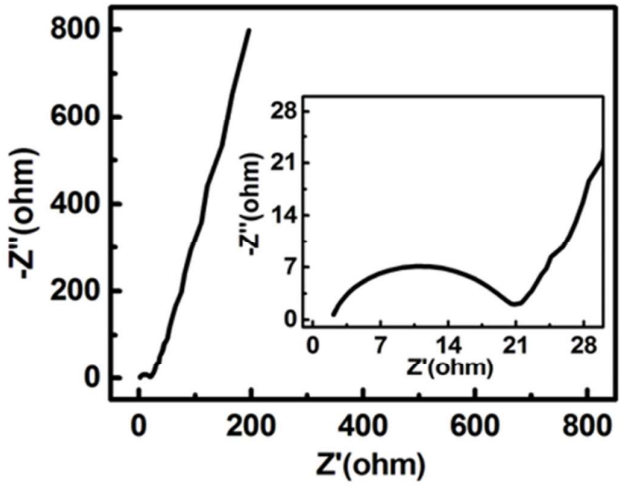

Fig. S4. EIS pattern of the CDMMC-based symmetric EC with 1 M $TEABF_4$/PC electrolyte. The inset for the corresponding high-frequency region of the EIS spectrum